Available online at www.sciencedirect.com
ScienceDirect
Trans. Nonferrous Met. Soc. China 33(2023) 1244−1257
Transactions of Nonferrous Metals Society of China
www.tnmsc.cn

Hydrodynamic simulation of metal droplet settlement in molten slag

Qin-meng WANG, Ming-xing HUANG, Shu-yang YAN, Song-song WANG, Qing-hua TIAN, Xue-yi GUO

School of Metallurgy and Environment, Central South University, Changsha 410083

Received 4 December 2021; accepted 12 April 2022

Abstract: A mathematical model of the metal droplet settlement process of smelting slag was established. The effect of interfacial tension between the metal and slag phases on the droplet settlement velocity and drag force under different viscosity models was studied. The results showed that the Laminar and RNG $k-\varepsilon$ turbulence models accurately predict the final settlement velocity of smaller diameter droplets. The interfacial tension affects the settlement velocity of the droplet, and the effect gradually increases as the droplet size is increased. The "RNG + CSS" model accurately describes the droplet settlement process and the change in the droplet settlement velocity. The drag force coefficient formula under coupling interfacial tension was derived with the established mathematical model and experimental data. This model reveals the mechanism of the settlement process of metal droplets in smelting slag and provides theoretical guidance for reducing the content of valuable metals in slag in actual production.

Key words: metal settlement; interfacial tension; viscosity model; clarification and separation; fluid dynamics

1 Introduction

Oxygen-enriched smelting technology usually uses high-concentration oxygen to be injected into the molten pool at high speed and vigorously stirs the melt to accelerate the smelting reaction [1,2]. At the same time, high-intensity stirring and high oxygen potential lead to preliminary clarification and separation of multiple phases. In the oxygen-enriched smelting process, the metal loss in slag is mainly caused by mechanical inclusion. Improving the settlement conditions of metal droplets in slag can effectively reduce the metal content in slag and improve the direct metal yield [3−5].

In the study of TONG et al [6], through numerical simulation based on the volume of fluid (VOF) model, combined with the experimental device for physical simulation, the mechanism of metal droplet formation and the effect of the filling rate on its droplet behavior were studied. LIU et al [7] developed a 3-D mathematical model coupled with a magneto-hydrodynamic (MHD) model, which was used to investigate droplet formation and drip. ZHOU et al [8] studied the influence of metal droplet size and interfacial tension on the metal droplet settlement velocity. The study showed that the larger the metal droplet size and the greater the interfacial tension were, the more conducive the separation of metal droplets and slag was. WANG et al [9] adjusted the content of components in slag to change the interfacial tension of the slag, which increased the interfacial tension between the slag and matte and ensured the excellent separation of the slag and metal droplets. NATSUI et al [10] studied the movement behavior of matte and slag by a dynamic model and found an increase in interfacial tension effects on the settlement time of metal droplets. LAN et al [11] applied a super-gravity field to the system to accelerate droplet settlement and found an increase in interfacial tension between the metal droplets and slag, hindering the polymerization of tiny droplets and droplet settlement. SUZUKI et al [12]

Corresponding author: Xue-yi GUO, Tel: +86-18570348015, E-mail: xyguo@csu.edu.cn
DOI: 10.1016/S1003-6326(23)66179-5

investigated the interfacial tension between the metal phase and the slag phase on the separation of metal droplets in the slag phase by studying the behavior of sulfur and oxygen in the slag at the interface between the metal and the slag phase. The results showed that impurities in metal droplets could be reduced by controlling the interfacial tension between the metal and slag phases. In addition, relevant studies [13,14] reported the influence of interfacial tension on the sedimentation process of metal droplets and derived the appropriate formulas for the critical radius of floating metal droplets. The above studies showed that interfacial tension has a complex effect on the settlement process of metal droplets in slag. However, few mechanisms of interfacial tension on the settlement of metal droplets have been proposed. Therefore, it is necessary to study the mechanism of interfacial tension.

In general, the settlement behavior of a single droplet in a viscous fluid can be treated according to Stokes flow, and the classic Stokes equation can solve the final settlement velocity of the droplet. However, in the settlement process of high viscosity fluid, there is a relative motion between the droplet and the surrounding fluid interface, leading to droplet deformation and the change in the drag coefficient, which further affects the droplet settlement process [15,16].

In this work, computational fluid dynamics is used to simulate the settlement process of metal droplets in molten slag, which breaks through the limitations of traditional experimental methods [17]. The physical model and mathematical model of the droplet are constructed by the fluid mechanics simulation software, and the influence of the interfacial tension on the droplet settlement is investigated. The formula for calculating the drag force of the related interfacial tension is derived, which has guiding significance for the research on the settlement of metal droplets in slag.

2 Experimental

2.1 Physical model

According to the experimental model device used in Ref. [18], the physical model was established. The specific size parameters are shown in Fig. 1.

The geometric model is a cube structure with a size of 100 mm × 100 mm × 150 mm. A droplet settlement area with a width of 10 mm is taken at the center of the cube to ensure that the ratio of the width of the droplet movement area to the width of the model wall is less than 0.1. At this time, the influence of the wall on the droplet settlement process can be ignored. The central area is locally encrypted to ensure the non-correlation of the grid. As shown in Fig. 1, the initial state of the droplet is static, and the shape of the droplet is spherical. Under the action of gravity, the droplet begins to settle and generates a drag force. The settlement velocity of the droplet gradually increases, and the final settlement speed is obtained when the power of the droplet is balanced. In this work, the droplet diameters were set to be 2, 4, 6, 8, and 10 mm, to clarify the influence of the droplet diameter on the sedimentation velocity.

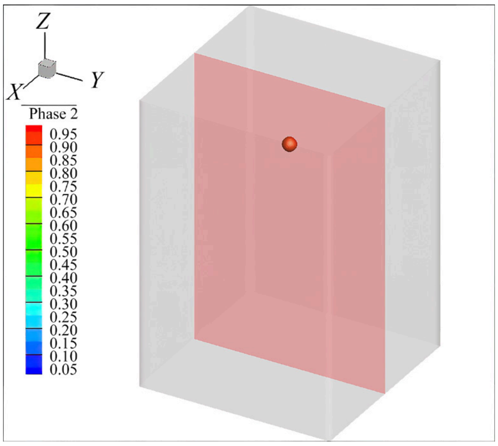

Fig. 1 Schematic diagram of geometric model of settlement system of metal droplets in slag

2.2 Mathematical model

The force analysis of the droplet shows that the droplet is subjected to gravity, buoyancy, and drag forces during the settlement process. When these three forces reach the balance, the final settlement velocity of the metal droplet can be obtained, which can be obtained by Stokes' equation:

$$v=\frac{gD^2(\rho_{\mathrm{m}}-\rho_{\mathrm{s}})}{18\mu_{\mathrm{s}}} \tag{1}$$

where v is the final settlement velocity of the droplet; g is the acceleration of gravity; D is the droplet diameter; ρ_{m} and ρ_{s} are the densities of the metal droplet and the slag, respectively; μ_{s} is the slag viscosity. The Reynolds number of the droplet is calculated as $Re\approx0.6$. The classical Stokes' equation was used to calculate the final settlement velocity of the metal droplet with a diameter of 10 mm. The Reynolds number of the droplet $Re\approx0.6$ is obtained, and the fluid flow can be seen as laminar flow. However, the relative motion between the droplet and the slag may cause turbulent motion at the two-phase interface. In this case, it is more accurate to use the turbulent viscosity instead of the slag viscosity to calculate the drag force.

Fluent software provides many turbulence models, including $k-\varepsilon$ model, $k-\omega$ model, Reynolds stress model, transition SST model, scale-adaptive simulation model, detached eddy simulation model, and large eddy simulation model, etc [19]. The RNG $k-\varepsilon$ turbulence model provides a differential equation that can calculate the turbulent viscosity at a low Reynolds number:

$$\frac{\partial}{\partial t}(\rho k)+\frac{\partial}{\partial x_i}(\rho k v_i)=\frac{\partial}{\partial x_j}\left(\alpha_k\mu_{\text{eff}}\frac{\partial k}{\partial x_j}\right)+ G_k+G_{\text{b}}-\rho\varepsilon-Y_M+S_k \tag{2}$$

$$\frac{\partial}{\partial t}(\rho\varepsilon)+\frac{\partial}{\partial x_i}(\rho\varepsilon v_i)=\frac{\partial}{\partial x_j}\left(\alpha_\varepsilon\mu_{\text{eff}}\frac{\partial \varepsilon}{\partial x_j}\right)+ C_{1\varepsilon}\frac{\varepsilon}{k}(G_k+C_{3\varepsilon}G_{\text{b}})-C_{2\varepsilon}\rho\frac{\varepsilon^2}{k}-R_\varepsilon+S_\varepsilon \tag{3}$$

where k is turbulent energy, ε is the turbulent dissipation rate, α_ε and α_k are the turbulent Prandtl number, μ_{eff} is the effective turbulent viscosity coefficient. G_k is the turbulent energy due to the mean velocity gradient, G_{b} is the turbulent energy due to buoyancy, Y_M is the effect of fluctuating expansion on the total dissipation rate in compressible turbulence, S_k and S_ε are the source terms, and $C_{1\varepsilon}$, $C_{2\varepsilon}$ and $C_{3\varepsilon}$ are constants.

The SST $k-\omega$ turbulence model considers the transport process of turbulent shear force in the definition of turbulent viscosity, which can accurately describe the flow separated from the smooth surface [20]. Therefore, in this work, the variation trend of droplet settlement velocity under three viscosity models was mainly considered: Laminar, RNG $k-\omega$ turbulence, and SST $k-\omega$ turbulence.

The VOF model provides two coupled surface tension models: the continuum surface force (CSF) model and the continuum surface stress (CSS) model. There is not much difference between the two models in describing the effect of surface tension, but the CSS model is mainly used for changing surface tension, so the CSS model was chosen in this work.

The classic Stokes' equation defines the drag force (F_{drag}) on a droplet as follows:

$$F_{\text{drag}}=3\pi\mu_{\text{s}}Dv \tag{4}$$

Based on this, RYZHENKOV et al [21] introduced a correction factor to the formula to accurately describe the drag force in the liquid−liquid two-phase system. The modified drag force, and the final settlement velocity of droplets are deduced as follows:

$$F_{\text{drag}}=2\pi\mu_{\text{s}}Dv\lambda \tag{5}$$

$$v=\frac{gD^2(\rho_{\text{m}}-\rho_{\text{s}})}{12\mu_{\text{s}}\lambda} \tag{6}$$

where λ is the correction factor. In this work, the simulated droplet sedimentation velocity is compared with the velocity calculated by Eq. (6) and the experimental data reported in Ref. [18] to determine the model's accuracy.

3 Boundary conditions and solution strategies

3.1 Boundary conditions

The pressure outlet boundary condition was adopted, and the gauge pressure was set to be 0 Pa; the nonslip boundary condition was adopted at the rest of the wall, and the standard wall equation was adopted in the near-wall area. In this work, the settlement process of metal droplets in molten slag was simulated using the data reported in Ref. [18]. The metal droplet was a nickel droplet, and the viscous fluid of Al−Ca−Si−O slag type was applied. The specific physical parameters are given in Table 1.

Table 1 Physical parameters of settlement system (T=1500 °C) [18]

Material	Density/ $(kg\cdot m^{-3})$	Viscosity/ (Pa·s)	Surface tension/ $(N\cdot m^{-1})$
Nickel metal droplet	7770	0.004	0.45
Slag II	2445	4.105	−

3.2 Solution strategies

The transient pressure-based separation implicit algorithm was adopted and the time step was adjusted according to calculation convergence. The maximum time step was 0.0002 s. The Euler model, the Laminar model, RNG $k-\varepsilon$ turbulence model, and SST $k-\omega$ turbulence model were adopted. Pressure−velocity coupling mode was applied, discretization format of the PRESTO method was used, the compressive method was selected for the volume fraction, and upwind form is selected for momentum equation.

4 Results and discussion

4.1 Effect of viscous model on settlement velocity

The trends of the droplet sedimentation velocity under the Laminar model, RNG $k-\varepsilon$ turbulence model, and SST $k-\omega$ turbulence model are investigated without considering the effect of interfacial tension. The final settlement velocity obtained by simulation is compared with the calculated one by Eq. (6) and the experimental data obtained in Ref. [18]. The results are shown in Fig. 2.

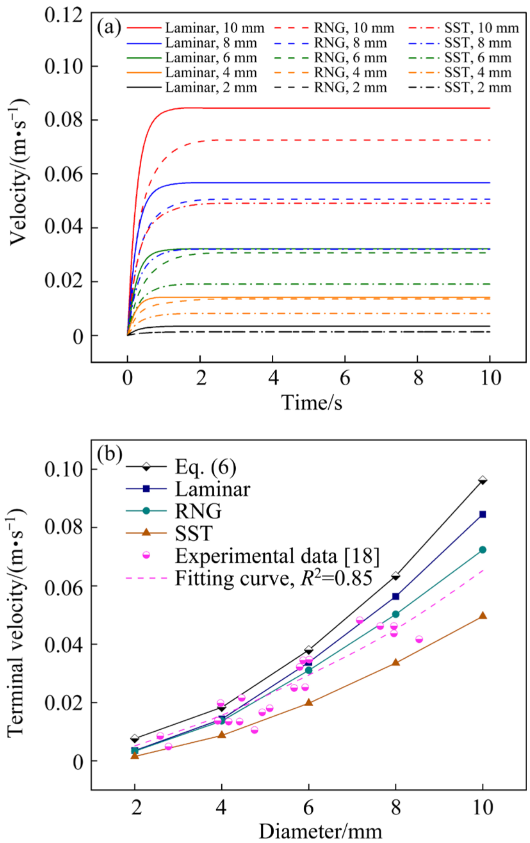

Fig. 2 Variation trend of droplet settlement velocity under different viscous models (a) and comparison of simulation results with calculated and experimental ones (b)

The droplet diameters were set as 2, 4, 6, 8, and 10 mm in three viscous models. The sedimentation velocity of metal droplets showed a gradual increasing trend and then reached a maximum value, indicating that the settlement process of the metal droplet in the molten slag is a variable acceleration process. The metal droplet moves downwards under gravity traction, and the viscous drag force opposite to the droplet motion direction is generated due to the slag viscosity. As the settlement velocity increases, the drag force on droplet gradually increases. When the drag force, gravity, and buoyancy reach a balance, the droplet obtains a maximum settlement velocity. The results of these three viscous models show that the final droplet settlement velocity is the minimum under the SST $k-\omega$ turbulence model and the maximum under the Laminar model.

The comparison results in Fig. 2(b) show differences among the simulation results obtained under three viscosity models, calculated by the formula, and the experimental results, and the difference becomes more evident with increasing droplet diameter. Compared with the experimental data, the final settlement velocity of the droplets under the SST $k-\omega$ turbulence model is smaller, and the velocity calculated by Eq. (6) is larger, which is not accurate enough to describe the change in the droplet settlement velocity in the system. The simulation results of the Laminar model and RNG $k-\varepsilon$ turbulence model are within the range of experimental data, which reflects the trend of droplet sedimentation velocity to some extent.

Equation (4) shows that the corresponding drag force coefficient determines the drag force on the droplet. The existing literature shows that the shape and deformation of the droplet have an important influence on the drag coefficient during droplet settlement. To clarify the changing trend of drag force under three viscous models, the shape change of droplets with different diameters at different settlement moments was studied, and the results are shown in Fig. 3.

It can be seen from Fig. 3 that the metal droplets of different diameters under three viscous models remain spherical and have no obvious deformation in the settlement process. The top of the droplet is concave, and the degree increases with the increase in diameter under the Laminar and RNG $k-\varepsilon$ turbulence models. The streamline

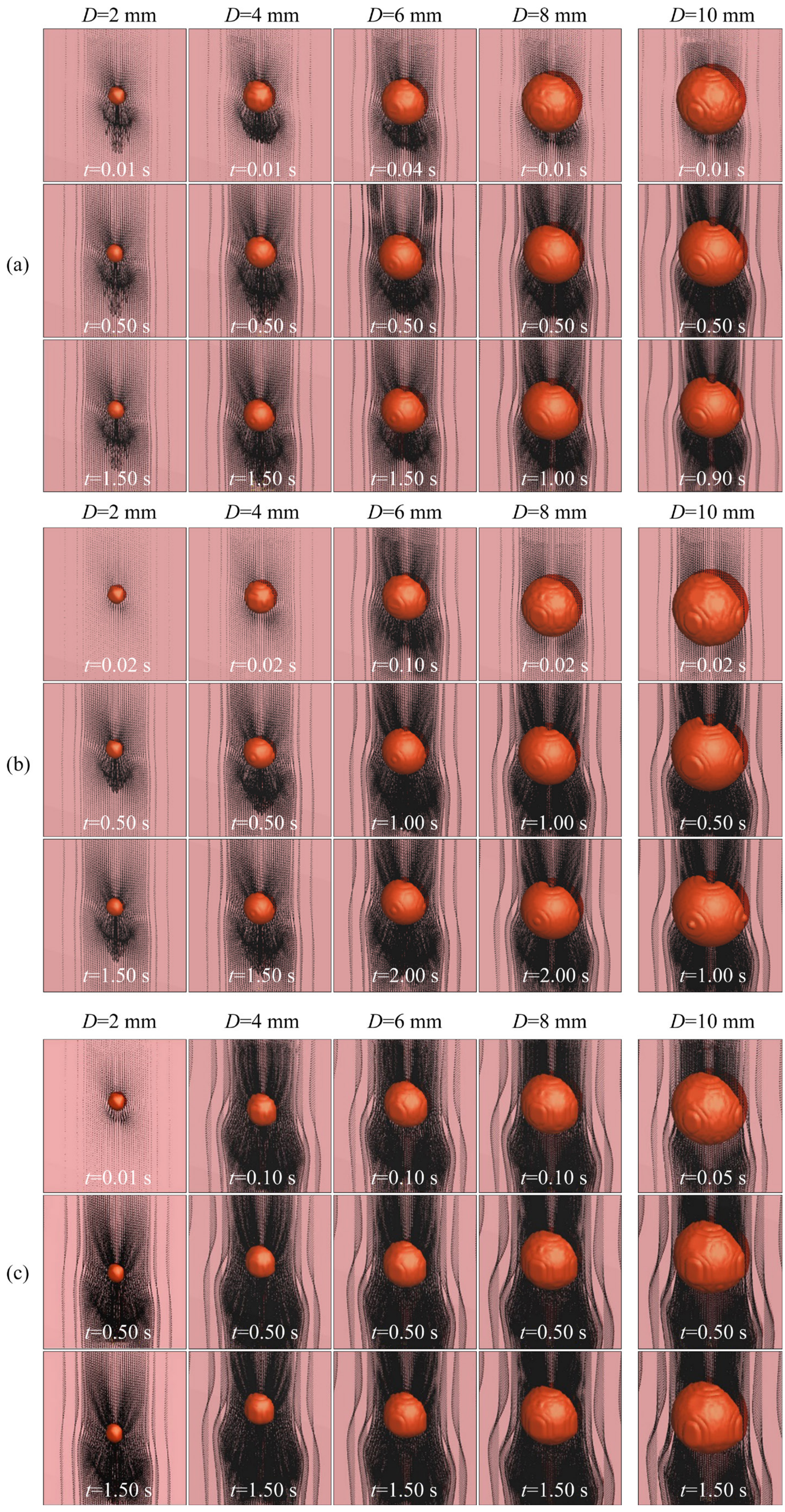

Fig. 3 Droplet shape change and streamline distribution under three viscosity models: (a) Laminar model; (b) RNG k−ε model; (c) SST k−ω model

distribution shows some differences in the velocity changes of the droplet under three viscous models. Under the Laminar model, the drag force on the droplet is small, and the streamline distribution of the droplet increases rapidly. The time it takes for the droplet to reach the final settlement velocity is the smallest. The droplet streamline distribution range is large, the energy transfer between the droplet and the surrounding fluid is significant under the RNG $k-\varepsilon$ turbulence and the SST $k-\omega$ turbulence models, and the droplet settlement velocity is lower than that under the Laminar model.

Figure 4 describes the changes in the distribution of the internal vector of the droplet under different viscosity models. It can be seen that the larger-diameter droplet still maintains a spherical shape under the Laminar and RNG $k-\varepsilon$ turbulence modes, but it splits due to the intrusion

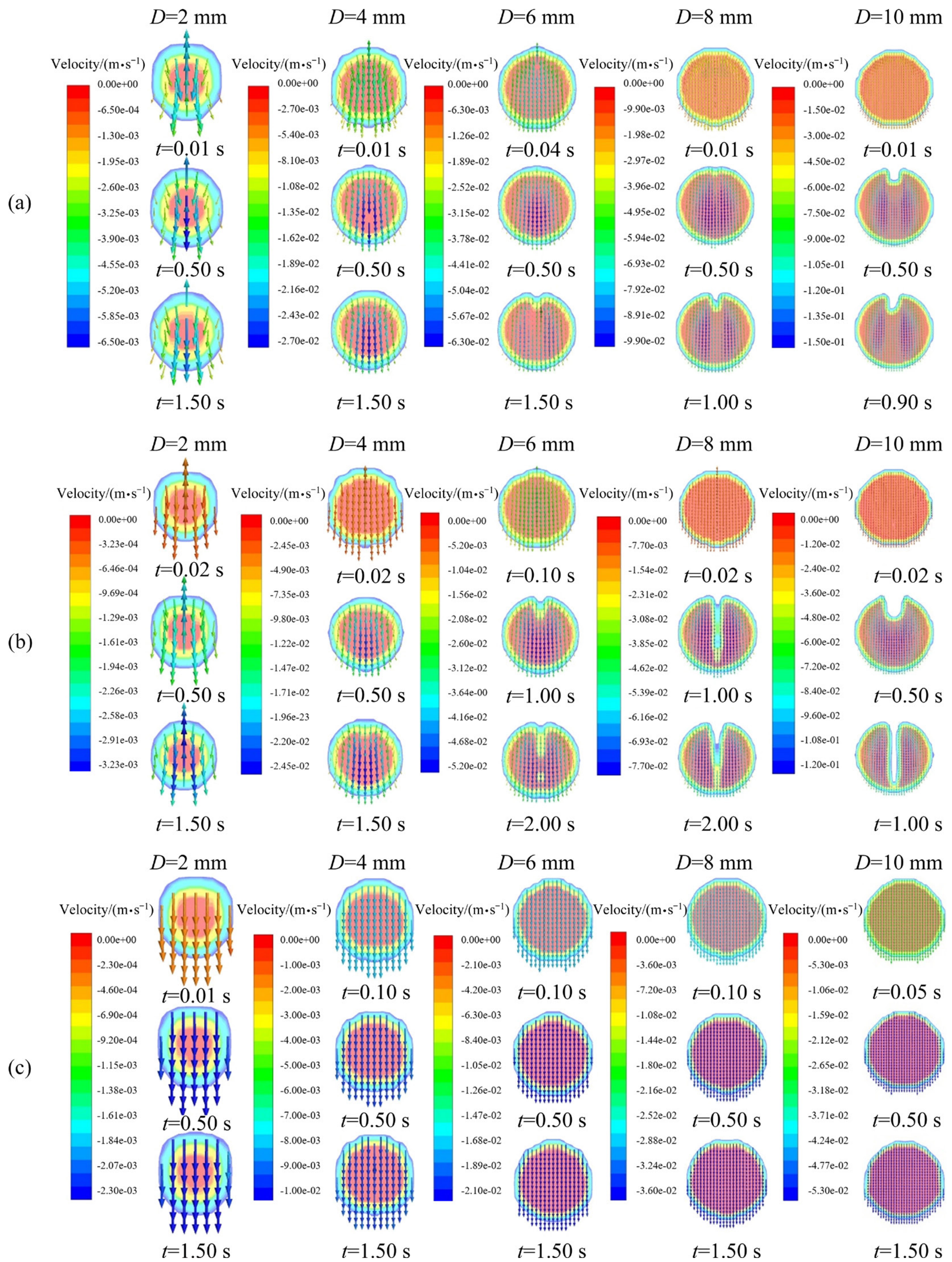

Fig. 4 Distribution of droplet internal vector under different viscosity models: (a) Laminar model; (b) RNG $k-\varepsilon$ model; (c) SST $k-\omega$ model

of the upper fluid into the droplet. The vector distribution shows that under the Laminar and RNG $k-\varepsilon$ turbulence models, the drag force is prominent at the interface between the drop and the surrounding fluid, and the droplet sedimentation velocity is small because the droplet directly contacts the slag. However, inside the droplet, because the viscosity of the droplets is much smaller than that of the slag, the drag force is small, the settlement velocity of the droplet is large, and the streamline distribution presents an apparent velocity gradient. Under the SST $k-\omega$ turbulence model, the internal vector of the droplet is single distribution, and there has no concave deformation on the top of the droplet, indicating that the model is not suitable for describing the droplet settlement process.

Figure 5 depicts the pressure distribution in the metal droplet settlement area under the Laminar and RNG $k-\varepsilon$ turbulence models. There is a pressure difference between the top and bottom of the droplet in the settlement process. With the increase in the droplet diameter, the pressure difference increases and eventually leads to the invasion of slag into the droplet, which may be the main reason for droplet deformation. By comparing Figs. 5(a) and 5(b), it is found that the pressure distribution in the droplet settlement area is more uniform under the RNG $k-\varepsilon$ turbulence model. In contrast, the pressure gradient under the Laminar model is more significant than that under the RNG $k-\varepsilon$ turbulence model, indicating that the RNG $k-\varepsilon$ turbulence model can better predict the pressure variation during the settlement process. In addition, the intrusion of slag into the inside of the droplet causes the liquid−liquid two-phase interaction and mutual

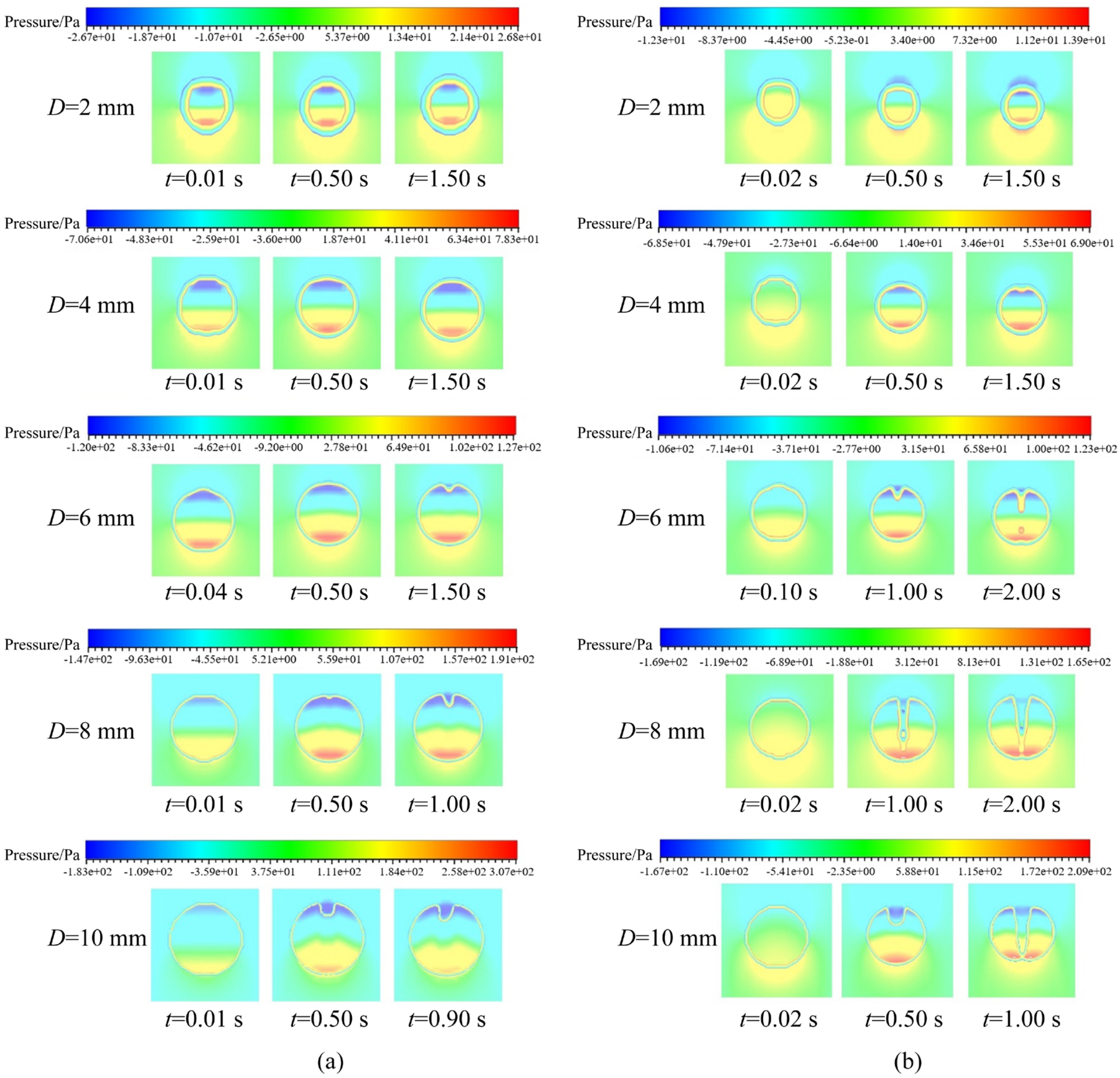

Fig. 5 Pressure distribution in droplet settlement region under Laminar model (a) and RNG $k-\varepsilon$ turbulence model (b)

intersection, and it is no longer suitable to regard the settlement system as laminar movement.

By comparing the simulation data, calculated data, and experimental data under three viscosity models, it can be seen that the Laminar and RNG $k-\varepsilon$ turbulence models can more accurately describe the effect of drag force on the droplet settlement velocity. When the droplet diameter is less than 6 mm, the Laminar and RNG $k-\varepsilon$ turbulence models can accurately predict the final droplet settlement velocity. When the droplet diameter is larger than 6 mm, the settlement velocity of the droplet stimulated by the RNG $k-\varepsilon$ turbulence model is closer to the last droplet settlement velocity obtained by the experiment.

4.2 Influence of interfacial tension on settlement velocity

According to the theory of fluid mechanics, when the Reynolds number of the droplet is large, the influence of interfacial tension on droplet shape becomes essential [22]. When the droplet diameter exceeds a specific critical value, the droplet begins to deform. Since the drag coefficient is directly related to the droplet shape, it is necessary to study the effect of interfacial tension on droplet settlement velocity. In this work, the CSS model is used to couple the interfacial tension with the Laminar and RNG $k-\varepsilon$ turbulence models, and the corresponding droplet sedimentation velocity curve is plotted.

As shown in Fig. 6, the droplet settlement velocity changes under the Laminar model are the same regardless of whether the CSS model is coupled. However, under the RNG $k-\varepsilon$ turbulence model, when the droplet diameter exceeds 6 mm, the settlement velocity obtained by the coupled CSS model is gradually different from that obtained by the uncoupled CSS model, and the difference increases with increasing droplet diameter. The results show that when the droplet settlement velocity is less than a specific critical value, the droplet drag coefficient remains unchanged. As the settlement velocity increases, the interaction between the droplet and slag is strengthened, and the droplet tends to deform. At this time, the interfacial tension plays a vital role in maintaining the droplet shape. Compared with the droplet without the CSS model, the droplet with the CSS model has a smaller drag force coefficient and a larger corresponding settlement velocity.

The simulation data obtained under the “Laminar + CSS” and “RNG + CSS” models are compared with experimental data and calculated data, as shown in Fig. 6(b). The results show that when the droplet diameter is less than 6 mm, the interfacial tension has little effect on the drag coefficient. When the droplet diameter is larger than 6 mm, the interfacial tension significantly affects the drag coefficient and increases as the droplet diameter increases. Compared with the experimental data, the data obtained by the “Laminar + CSS” and “RNG + CSS” models are within the practical range. It can be considered that the “Laminar + CSS” model and the “RNG + CSS” model can accurately describe the droplet settlement process in the studied system.

Figure 7 shows the internal vector distribution of the droplet under the “Laminar + CSS” model and the “RNG + CSS” model. By comparing Fig. 4 with Fig. 8, it can be seen that there is a significant

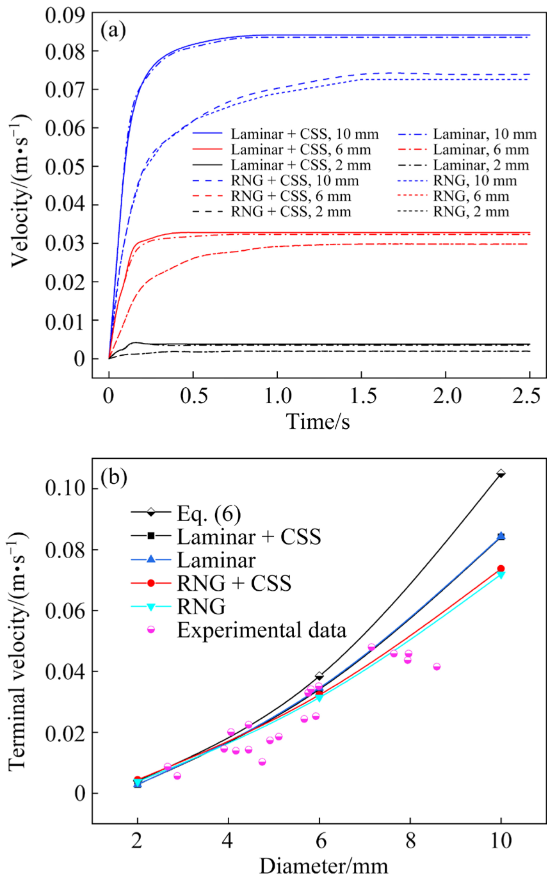

Fig. 6 Curves of droplet settlement velocity under viscous model coupled with CSS model (a), and comparison of simulation results with calculated and experimental results under “Laminar + CSS” and “RNG + CSS” models (b)

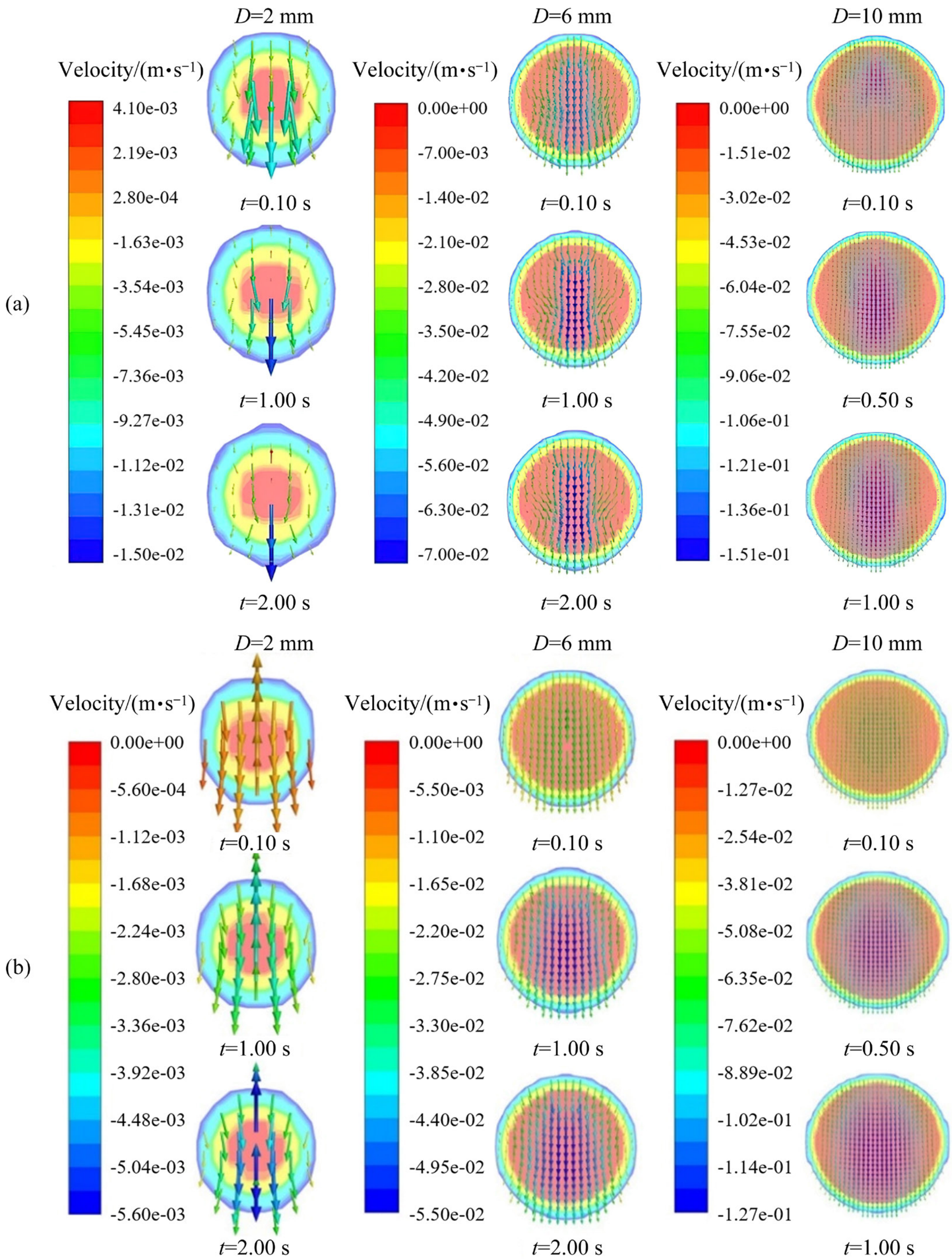

Fig. 7 Vector distribution of droplets under different viscous models coupled with CSS model: (a) "Laminar + CSS" model; (b) "RNG + CSS" model

difference between the droplet shapes of the coupled CSS model and those of the uncoupled model. The droplet of the coupled CSS model has no slag intrusion phenomenon, and the droplet only slightly deforms. This shows that the interfacial tension plays a positive role in maintaining the droplet's shape. The interfacial tension can inhibit the invasion of the surrounding fluid into the droplet and increase the droplet settlement velocity. The vector distribution inside the droplet indicates that the fluid in the central region moves in the opposite direction of settlement. The reason may be that the smaller diameter droplet is significantly disturbed in the settlement process, and the fluid inside the droplet circulates.

Figure 8 describes the pressure distribution during droplet settlement under the "Laminar + CSS" and "RNG + CSS" models. The results show

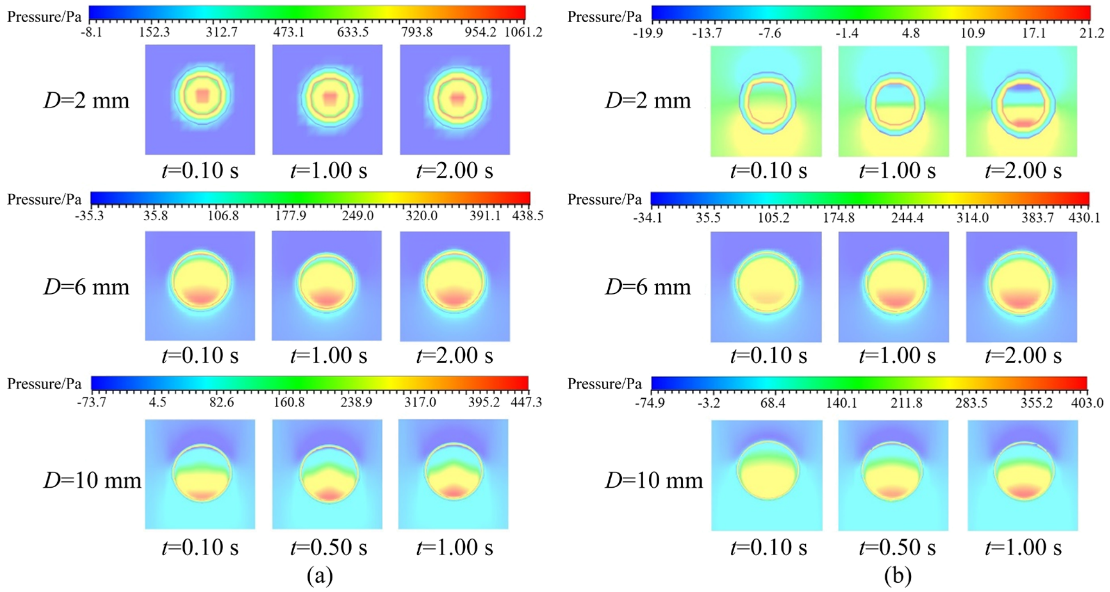

Fig. 8 Pressure distribution in droplet settlement region under "Laminar + CSS" model (a) and "RNG + CSS" model (b)

that when the droplet diameter is 2 mm, the internal pressure distribution of the droplet under the "Laminar + CSS" model is very different from that of the "RNG + CSS" model, which fails to describe the pressure change accurately. When the diameter is 6 or 10 mm, the pressure distribution under the two models is the same. As the metal droplet accelerates in the process of settlement, the pressure inside the droplet changes with increasing settlement speed. In this regard, the "Laminar + CSS" model cannot accurately describe the droplet pressure trend over time, while the "RNG + CSS" model can accurately describe the pressure change. In addition, it can be predicted that with a further increase in the droplet diameter, the pressure difference between the top and bottom of the droplet continues to increase. When the pressure difference increases to a specific value, the interfacial tension is not enough to maintain the original shape of the droplet, and the droplet deforms and splits.

In conclusion, the interfacial tension between the metal droplet and slag plays a vital role in maintaining the droplet shape. With increasing droplet diameter, the effect of interfacial tension on the droplet settlement velocity gradually increases. The "RNG + CSS" model can more accurately describe the droplet sedimentation process and the change in the droplet settlement velocity while considering the interfacial tension.

4.3 Improvement of empirical formula of drag coefficient

In general, the settlement of metal droplet in a viscous fluid is subjected to gravity (F_G), buoyancy (F_B), and drag force (F_D). At the initial settlement stage, the static metal droplet accelerates under the action of gravity, and the drag force is generated. According to the law of force balance, the droplet obtains the final settlement velocity when the resultant force reaches equilibrium. At this point, the force equilibrium equation can be written as

$$F_D=F_G-F_B \tag{7}$$

Among them,

$$F_G=\frac{1}{6}\pi\rho_m gD^3 \tag{8}$$

$$F_B=\frac{1}{6}\pi\rho_s gD^3 \tag{9}$$

Equation (7) can be converted into

$$F_D=C_D\cdot\frac{1}{2}\rho_s v^2\cdot\frac{1}{4}\pi D^2 \tag{10}$$

where C_D is the drag coefficient. According to the classic Stokes' law, the main parameters affecting the drag force are the droplet diameter D, the slag density ρ_s, the slag viscosity μ_s, and the final settlement velocity v. Therefore, F_D can be regarded as a correlation function of the above parameters:

$$F_D=f(D,\ \rho_s,\ \mu_s,\ v) \tag{11}$$

The corresponding drag force equation can be derived from Buckingham's π theorem. In Eq. (11), four physical variables can be expressed as corresponding relations by three independent physical units (M, L, T). Buckingham's π theorem shows that Eq. (11) can be converted to an equivalent relationship with only two dimensionless parameters. In this section, the variables D, ρ_s, and v are selected as independent physical units, and the corresponding dimensionless parameters are

$$\pi_1 = \frac{F_D}{D^{a_1}\rho_s^{b_1}v^{c_1}} \tag{12}$$

$$\pi_2 = \frac{\mu_s}{D^{a_2}\rho_s^{b_2}v^{c_2}} \tag{13}$$

According to the analysis of the dimensional harmony principle, the indices a_1, b_1, c_1 and a_2, b_2, c_2 are solved as follows:

$a_1=2$, $b_1=1$, $c_1=2$, $a_2=1$, $b_2=1$, $c_2=1$

Therefore,

$$\pi_1 = \frac{F_D}{D^2\rho_s v^2},\quad \pi_2 = \frac{\mu_s}{D\rho_s v} = \frac{1}{Re} \tag{14}$$

where Re is the Reynolds number of the droplet. Thus, π_1 can be expressed as a function of π_2:

$$\frac{F_D}{D^2\rho_s v^2} = f(Re) \tag{15}$$

According to Eq. (10), Eq. (15) can be transformed into

$$F_D = \frac{8}{\pi} f(Re)\cdot\frac{1}{2}\rho_s v^2\cdot\frac{1}{4}\pi D^2 \tag{16}$$

The drag coefficient can be expressed as

$$C_D = \frac{8}{\pi} f(Re) \tag{17}$$

The droplet drag coefficient is related to the Reynolds number. In Stokes flow, the drag force coefficient is usually given as [23]

$$C_D = \frac{24}{Re} \tag{18}$$

Similarly, according to the modified drag force (Eq. (6)), the corresponding modified drag force coefficient is

$$C_D' = \frac{16\lambda}{Re} \tag{19}$$

The comparison result in Fig. 6(b) shows a deviation between the simulation results and the calculated and experimental results, which is caused by the influence of the interfacial tension on the fluid shape. Therefore, it is necessary to consider the change in the droplet drag coefficient under interfacial tension. By taking the interface tension parameter σ into the drag force equation, Eq. (11) can be rewritten as

$$F_D = f(D,\ \rho_s,\ \mu_s,\ v,\ \sigma) \tag{20}$$

A new dimensionless parameter π_3 is obtained:

$$\pi_3 = \frac{\sigma}{Dv^2\rho_s} \tag{21}$$

The dimensionless parameter π_1 can be expressed as

$$\frac{F_D}{D^2\rho_s v^2} = k_1\pi_2^{k_2}\pi_3^{k_3} \tag{22}$$

Among them, k_1, k_2, and k_3 are unknown constants. By combining π_2 and π_3, the parameter π_4 can be obtained:

$$\pi_4 = \pi_2\cdot\pi_3^{-1} = \frac{\mu_s v}{\sigma} \tag{23}$$

π_4 is the droplet capillary number C_a. Thus, π_1 can be seen as a function of C_a:

$$\frac{F_D}{D^2\rho_s v^2} = k_4 C_a^{k_5} \tag{24}$$

k_4 and k_5 are unknown constants. According to Eq. (17), the corresponding drag force coefficient C_D'' equation considering the interfacial tension coefficient is

$$C_D'' = \frac{8}{\pi}\cdot k_4 C_a^{k_5} = k_6 C_a^{k_5} \tag{25}$$

where k_6 is an unknown constant.

Based on the simulation results under the "RNG + CSS" model, the calculated results of Eq. (19), and the experimental data, the change curves of the droplet drag force coefficients with different diameters are calculated, as shown in Fig. 9.

As shown in Fig. 9, within the allowable range of experimental error, results by Eq. (19) and the drag force coefficient calculated from the simulation results of the "RNG + CSS" model both show good agreement. However, combined with the final droplet velocity change shown in Fig. 6(b), it can be seen that the drag force coefficient C_D'' calculated from the simulation results of the

"RNG + CSS" model can more accurately describe the droplet settlement velocity change trend. By combining the data of C_D'', curve fitting on Eq. (25) is performed by the least square method, and the relevant parameters obtained are given in Table 2.

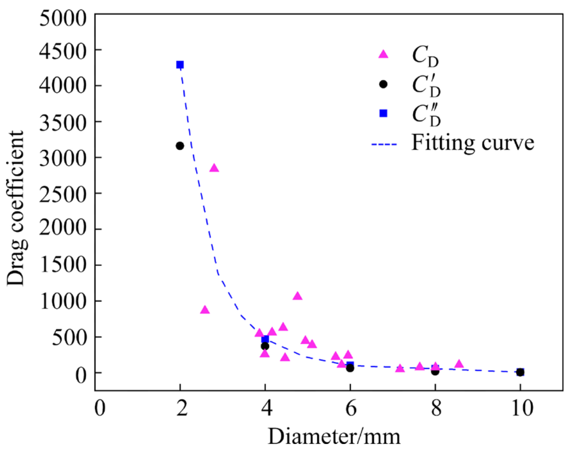

Fig. 9 Variation of drag coefficient with different droplet diameters (C_D is calculated according to the experimental data [18]; C_D' is calculated according to Eq. (19); C_D'' is based on simulation results of "RNG + CSS" model)

Table 2 Fitting parameters of Eq. (25)

Equation	k_5	k_6	R^2
$C_D''=k_6C_a^{k_5}$	−1.367	40.671	0.998

4.4 Data verification

To further verify the applicability of the mathematical model and drag force coefficient calculation (Eq. (25)) used in this work, another settlement system (Fe-slag settlement system) in Ref. [18] was combined for verification. The metal droplet used in the system is a saturated iron droplet, and the slag is of the Al−Ca−Si−O slag type. Specific physical parameters are given in Table 3.

Table 3 Physical parameters of settlement system (T=1450 °C) [24]

Material	Density/ $(kg\cdot m^{-3})$	Viscosity/ $(Pa\cdot s)$	Surface tension/$(N\cdot m^{-1})$
Iron metal droplet	6770	0.0058	0.15
Slag I	2660	2.21	–

The "RNG + CSS" model is used to simulate the Fe-slag settlement system, and the results are compared with the calculation results of the improved equation and the experimental results, as shown in Fig. 10.

Figure 10 shows that for tiny diameter metal droplets, the calculation results of the enhanced formula and the simulation results of the "RNG + CSS" model are in good agreement with the experimental results. For large diameter metal droplets (when the diameter is larger than 10 mm), the "RNG + CSS" model predicts the settlement velocity of droplets more accurately.

Equation (25) is used to calculate the drag force coefficient of the Fe-slag system under the "RNG + CSS" model and it is compared with the drag force coefficient calculated from the experimental data and the drag force coefficient calculated by the improved formula. The results are shown in Fig. 11.

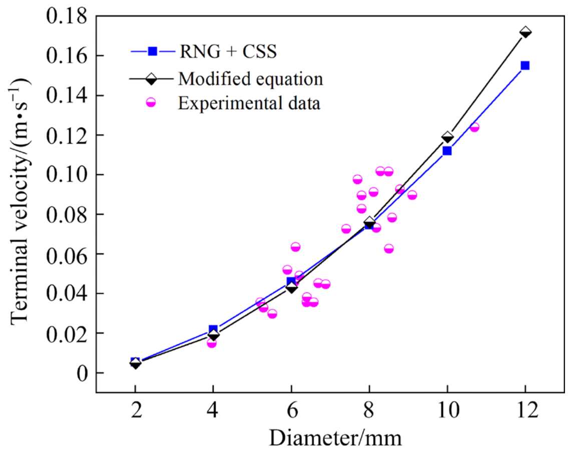

Fig. 10 Comparison of settlement velocity of Fe-slag system under three different methods

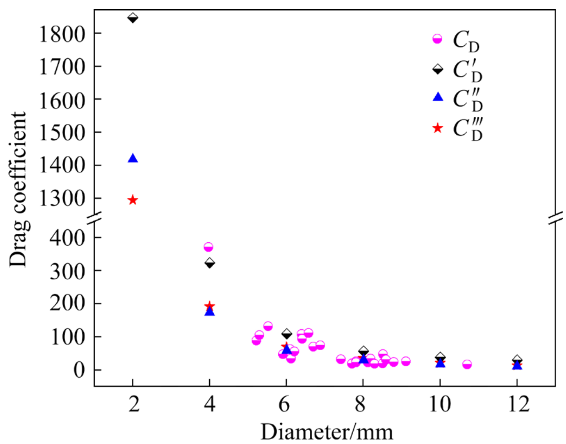

Fig. 11 Comparison of drag coefficients under different droplet diameters (C_D is calculated according to experimental data; C_D' is calculated according to Eq. (19); C_D'' is based on the simulation results of the "RNG + CSS" model; C_D''' is calculated according to Ref. [18])

As shown in Fig. 11, due to the difficulty in obtaining iron droplets with a diameter less than 2 mm in the experimental process and the significant measurement error, the settlement velocity data of the droplets with a diameter less than 2 mm were not given in the literature. However, according to the overall drag force coefficient variation trend, the drag force coefficient calculated from Eq. (25) agrees with the experimental data for predicting the drag coefficient of different metal droplets. The results show that the interfacial tension between the droplet and the slag has an essential effect on the droplet settlement process under the metal droplet−slag system studied in this work, and the corresponding drag force coefficient can be calculated according to $C''_D=40.671(C_a)^{-1.367}$.

5 Conclusions

(1) For smaller-diameter droplets, the Laminar model and RNG $k-\varepsilon$ turbulence model can accurately predict the final settlement velocity of the droplets. When the droplet diameter is larger than 6 mm, the simulated droplet settlement velocity in the RNG $k-\varepsilon$ turbulence model is closer to the final settlement velocity of the experimental droplet.

(2) Interfacial tension affects the droplet settlement velocity, and with increasing droplet diameter, the effect of interfacial tension on the droplet settlement velocity increases. The “RNG + CSS” model can more accurately describe the droplet settlement process and the change in the droplet settlement velocity while considering the interfacial tension.

(3) By combining the mathematical model and experimental data, the formula for calculating the drag force coefficient under the action of the coupling interfacial tension is derived: $C''_D=40.671(C_a)^{-1.367}$.

Acknowledgments

The authors are grateful for the financial supports from the National Natural Science Foundation of China (Nos. 51904351, 51620105013, U20A20273), the National Key R&D Program of China (No. 2019YFC1907400), the Science and Technology Innovation Program of Hunan Province, China (No. 2021RC3005), the Major Technological Innovation Projects of Shandong Province, China (No. 2019JZZY010404), and the Innovation Driven Program of Central South University, China (No. 2020CX028).

References

[1] GUO Xue-yi, TIAN Miao, WANG Song-song, YAN Shu-yang, WANG Qin-meng, YUAN Zhong-sen, TIAN Qing-hua, TANG Ding-xuan, LI Zhong-chen. Element distribution in oxygen-enriched bottom-blown smelting of high-arsenic copper dross [J]. JOM, 2019, 71(11): 3941−3948.

[2] WANG Qin-meng, GUO Xue-yi, TIAN Qing-hua. Copper smelting mechanism in oxygen bottom-blown furnace [J]. Transactions of Nonferrous Metals Society of China, 2017, 27(4): 946−953.

[3] ZHANG Jiang-liang, YANG Xu, ZHANG Jian-kun, CHEN Yong-qiang, ZHANG Li-feng, WANG Chen-yan. Influence of slag contents on sedimentation separation of slag and matte at high temperature [J]. The Chinese Journal of Nonferrous Metals, 2019, 29(8): 1712−1720. (in Chinese)

[4] SUNGHWAN J, SPAGNOLIE S E, PARIKH K, SHELLE M. Periodic sedimentation in a Stokesian fluid [J]. Physical Review E: Statistical, Nonlinear, and Soft Matter Physics, 2006, 74(3): 1−4.

[5] WANG Qin-ming, WANG Song-song, TIAN Miao, TANG Ding-xuan, TIAN Qing-hua, GUO Xue-yi. Relationship between copper content of slag and matte in the SKS copper smelting process [J]. International Journal of Minerals Metallurgy and Materials, 2019, 26(3): 301−308.

[6] TONG Wen-jie, LI Wan-ming, ZANG Xi-min, LI Hua-bing, JIANG Zhou-hua, HAN Yu. Droplet formation and dripping behavior during the electroslag remelting process with two series-connected electrodes [J]. Metals, 2020, 10(3): 1−20.

[7] LIU Shuang, HE Zhu, HUI Cai, WANG Qiang, LI Bao-kuan. Numerical simulation of the formation and the dripping of droplet in the electroslag remelting process [J]. Thermal Science, 2017, 21(3): 1241−1250.

[8] ZHOU Ye-lian, DENG Zhi-yin, ZHU Miao-yong. Numerical simulation on separation process of liquid inclusion at steel−slag interface [J]. Iron and Steel, 2018, 53(7): 31−37. (in Chinese)

[9] WANG Guo-hua, CUI Ya-ru, LI Xiao-ming, YANG Shu-feng, ZHAO Jun-xue, TANG Hong-liang, LI Xu-teng. Molecular dynamics simulation on microstructure and physicochemical properties of $Fe_xO-SiO_2-CaO-MgO$−“NiO” slag in nickel matte smelting under modulating CaO content [J]. Minerals, 2020, 10(2): 1−15.

[10] NATSUI S, NASHIMOTO R, KUMAGAI T, KIKUCHI T, SUZUKI R O. An SPH study of molten matte–slag dispersion [J]. Metallurgical and Materials Transactions B, 2017, 48(3): 1792−1806.

[11] LAN Xi, GAO Jin-tao, HUANG Zili, GUO Zhan-cheng. Rapid separation of copper phase and iron-rich phase from copper slag at low temperature in a super-gravity field [J].

Metallurgical and Materials Transactions B, 2018, 49(3): 1165−1173.

[12] SUZUKI M, NAKAMOTO M, TANAKA T, TSUKAGUCHI Y, MISHIMA K, HANAO M. Effect of sulfur in slag on dynamic change behavior of liquid iron/molten slag interfacial tension: Fundamentals of high temperature processes [J]. ISIJ International, 2020, 60(11): 2332−2338.

[13] ELLIOTT J F, MOUNIER M. Surface and interfacial tensions in copper matte-slag systems, 1200 °C [J]. Canadian Metallurgical Quarterly, 2013, 21(4): 415−428.

[14] KAPTAY G. Discussion of “microscale simulation of settler processes in copper matte smelting” [J]. Metallurgical and Materials Transactions B, 2001, 32(3): 555−557

[15] NOROUZI M, ABDOLNEZHAD H, MANDANI S. An experimental investigation on inertia motion and deformation of Boger drops falling through Newtonian media [J]. Meccanica, 2019, 54(3): 473−490.

[16] WANG Zhi-bin, SUN Tian-li, YANG Zhong-wei, ZHU Guo, SHI Hong-yan. Interactions between two deformable droplets in tandem fixed in a gas flow field of a gas well [J]. Applied Sciences, 2021, 11(23): 11220.

[17] ZHANG Jian-ping, JOHNSON W, PLIKAS T. Application of computational fluid dynamics for solving ventilation problems in metallurgical industrial processes [J]. International Journal of Ventilation, 2017, 16(3): 200−212.

[18] IWAMASA P K, FRUEHAN R J. Separation of metal droplets from slag [J]. ISIJ International, 1996, 36(11): 1319−1327.

[19] MENTZONI F, ERTESVG I S, RIAN K E, KLEIVELAND R N. Numerical modeling of turbulence above offshore helideck−Comparison of different turbulence models [J]. Journal of Wind Engineering and Industrial Aerodynamics, 2015, 141: 49−68.

[20] SHAO Jie, LI Xiao-hua, GUO Zhen-jiang, LIU Rui-jing, TIAN Xiao-liang. Application of $k-\omega$ turbulence models on numerical simulation of frictional drag [J]. Journal of Qingdao University (E&T), 2016, 31(1): 120−124. (in Chinese)

[21] RYZHENKOV A N, YAROSHEVSKII S L, ZAMURUEV V P, POPOV V E, AFANAS’EVA Z K. Study of a blast-furnace smelting technology which involves the injection of pulverized-coal fuel, natural gas, and an oxygen- enriched blast into the hearth [J]. Metallurgist, 2006, 50(5/6): 235−240.

[22] MOHAMAD M S, DOVER C M, SEFIANE K. Experimental investigation of drag coefficient of free-falling deformable liquid gallium droplet [J]. The European Physical Journal Applied Physics, 2018, 84(1): 1−6.

[23] MORSI S A, ALEXANDER A J. An investigation of particle trajectories in two-phase flow systems [J]. Journal of Fluid Mechanics, 1972, 55(2): 193−208.

[24] MONAGHAN J J, GINGOLD R A. Shock simulation by the particle method SPH [J]. Journal of Computational Physics, 1983, 52(2): 374−389.

熔渣中金属液滴沉降过程流体力学模拟

王亲猛，黄明星，闫书阳，王松松，田庆华，郭学益

中南大学 冶金与环境学院，长沙 410083

摘　要：建立熔炼渣中金属液滴沉降过程的数学模型，研究不同粘性模型下金属/熔渣界面张力对液滴沉降速度以及拖曳力的影响。结果表明：对于较小直径的液滴，Laminar 模型和 RNG $k-\varepsilon$ 湍流模型能够准确预测液滴最终沉降速度；界面张力对液滴沉降速度有影响，且影响作用随着液滴尺寸增大而逐渐增大；“RNG+CSS”模型可以准确描述液滴沉降过程和液滴沉降速度的变化。结合数学模型和实验数据，推导出耦合界面张力作用下拖曳力系数计算公式。该模型揭示熔炼渣中金属液滴沉降过程机理，为实际生产中降低渣中有价金属含量提供理论指导。

关键词：金属沉降；表面张力；粘性模型；澄清分离；流体动力学

(Edited by Bing YANG)